

Luminescence spectroscopy of matrix-isolated atomic manganese: Excitation of the “forbidden” $a^6D_J \leftrightarrow a^6S$ transitions

Martin A. Collier,^{a)} Maryanne C. Ryan, and John G. McCaffrey^{b)}

Department of Chemistry, National University of Ireland—Maynooth, Maynooth, County Kildare, Ireland

(Received 10 January 2005; accepted 26 May 2005; published online 2 August 2005)

Laser-induced excitation spectra recorded for the electric-quadrupole $3d^64s a^6D_J \leftarrow 3d^54s^2 a^6S_{5/2}$ transitions of atomic Mn, allow assignment of the red emission features, previously observed in Mn/RG (RG=Ar, Kr and Xe) matrices with resonance $3d^54s4p z^6P_{5/2} \leftarrow 3d^54s^2 a^6S_{5/2}$ excitation, to the metastable $a^6D_{9/2}$ state. Narrow excitation bands recorded for the red site in the Mn/Kr system allow identification of all five spin-orbit levels ($J=1/2, 3/2, 5/2, 7/2$ and $9/2$) in the a^6D state. The coincidence of the lowest energy excitation band and the observed 585.75 nm ($17\,072\text{ cm}^{-1}$) emission band of atomic Mn in Kr matrices, yielded a definitive assignment of this emission to a transition from the $J=9/2$ spin-orbit level. Temperature dependent emission scans lead to the identification of the zero phonon line for the $a^6D_{9/2} \rightarrow a^6S_{5/2}$ transition at 585.75 nm. The identified matrix-shift of $+20\text{ cm}^{-1}$ allows an assessment of the extent of the ground state stabilization in the red (2°) site of atomic Mn isolation in solid Kr. Emission produced with direct a^6D state excitation yielded both the 585.75 and 626 nm features. The former band arises for Mn atoms occupying the red site—the latter from blue site occupancy in solid Kr. The excitation linewidths recorded for these two sites differ greatly, with the blue site yielding a broad featureless profile, in contrast to the narrow, structured features of the red site. The corresponding red site $a^6D_J \leftrightarrow a^6S_{5/2}$ transitions in Ar and Xe matrices are broader than in Kr—a difference considered to originate from the site sizes available in these hosts and the interatomic Mn·RG potentials. The millisecond decay times recorded for the red emission bands in the Mn/RG systems are all much shorter than the 3 s value predicted for the gas phase $a^6D_{9/2} \rightarrow a^6S_{5/2}$ transition. This enhancement allows optical pumping of the forbidden $a^6D_J \leftrightarrow a^6S$ transitions with low laser powers when atomic manganese is isolated in the solid state. However all the emission decays are complex, exhibiting triple exponential decays. This behavior may be related to the dependence of the excitation linewidths on the J value, indicating removal of the J degeneracy due to weak matrix-induced, crystal field splitting. © 2005 American Institute of Physics. [DOI: 10.1063/1.1961531]

I. INTRODUCTION

The luminescence excitation¹ and emission² spectroscopy reported by our group for atomic manganese isolated in solid Ar, Kr and Xe, produced with excitation of the $3d^54s4p z^6P_{5/2} \leftarrow 3d^54s^2 a^6S_{5/2}$ transition, revealed emission bands in the red spectral region that were only tentatively assigned to the $a^6D_{9/2} \rightarrow a^6S_{5/2}$ transition. To establish the validity of these assignments, excitation scans in the region of the gas phase³ $3d^64s a^6D_J \leftarrow 3d^54s^2 a^6S_{5/2}$ transitions of atomic Mn (centred around 573 nm) were sought for the red emission bands. The extreme weakness of the forbidden $a^6D \leftarrow a^6S$ transition relative to the allowed $z^6P \leftarrow a^6S$ transition, is indicated in Fig. 1 which lists the known gas phase radiative lifetimes (τ) as 3.4 s and 52 ns, respectively, for the two transitions.^{4–6} The weak oscillator strength of the electric-dipole forbidden transition from the ground $a^6S_{5/2}$ state to the a^6D_J states required a high intensity excitation source; hence a pulsed laser was used. From the shortened decay times observed in our earlier matrix work² for the red emission features, it is, however, expected, that the “forbid-

den” $a^6D_J \leftarrow a^6S$ transitions will be much easier to pump under solid state conditions than in the gas phase. This is indeed the case, as is demonstrated ahead with the moderate laser powers employed to obtain emission signals with acceptable signal-to-noise (S/N) ratios.

The excitation spectroscopy recorded for the $z^6P \leftarrow a^6S$ transition, reported in Ref. 1 and hereafter referred to as Paper I, indicated the existence of a pair of sites for atomic Mn isolation in solid Ar and Kr and a single, thermally stable site in Xe. As revealed by the linear dependence of the z^6P state matrix shifts with the polarizability of the rare gas host, the blue sites in Ar, Kr and Xe were attributed, from the recorded excitation spectra, to single vacancy occupancy of atomic manganese. A similar analysis of the red site features in Ar and Kr lead to the proposal of tetravacancy occupancy for this site. The observation in Ref. 2 (Paper II) of very different emission for the red and blue sites, leads to the identification of strong site-specificity for the relaxation of excited atomic Mn isolated in the solid rare gases. A short review of the spectral characteristics and state assignments of the emission bands in the red spectral region now follows.

Mn/Xe was found to be the simplest of the Mn/RG matrix systems exhibiting only a single, thermally stable site of

^{a)}Present address: Laboratoire Francis Perrin, CEA Saclay, France.

^{b)}Electronic mail: john.mccaffrey@nuim.ie

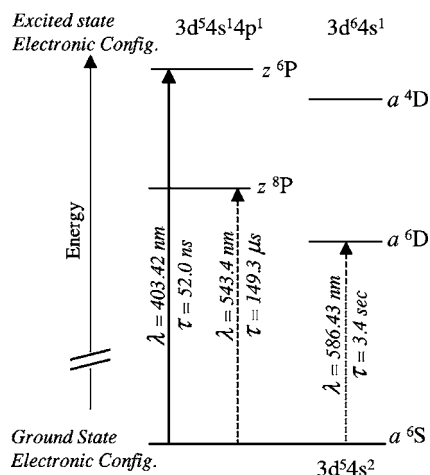


FIG. 1. An energy level diagram for gas phase atomic manganese showing the states that exist at energies lower than the $z^6P_{5/2}$ state reached by a fully allowed electric-dipole transition from the ground $a^6S_{5/2}$ state. The transition to the $z^6P_{5/2}$ state as well as the forbidden $z^8P_{5/2}$ and $a^6D \leftrightarrow a^6S$ transitions, indicated by the arrows, occur at $24\,788 \text{ cm}^{-1}$ (403.42 nm), $18\,402 \text{ cm}^{-1}$ (543.40 nm) and $17\,451 \text{ cm}^{-1}$ (573.03 nm), respectively (Ref. 3). The gas phase radiative lifetimes (Refs. 4–6) (τ) for these transitions are also indicated, revealing the very large difference between the electric-dipole allowed $z^6P \leftrightarrow a^6S$ transition and the forbidden $a^6D \leftrightarrow a^6S$ transition.

isolation in absorption and excitation spectra, which is blue-shifted with respect to the gas phase $z^6P_{5/2} \leftarrow a^6S_{5/2}$ transition. The resulting single emission band, located at 620 nm ($16\,129 \text{ cm}^{-1}$) with a linewidth of 240 cm^{-1} full width at half-maximum (FWHM), exhibits a matrix shift of -926 cm^{-1} from the gas phase $a^6D_{9/2} \leftrightarrow a^6S_{5/2}$ transition. The spectral position, asymmetric band shape and the millisecond decay time, suggested assignment of the 620 nm emission to the $a^6D_{9/2} \rightarrow a^6S_{5/2}$ transition. However, the absence of emission bands from the z^8P state (see Fig. 1) and the broad lineshape did not completely preclude an alternative $z^8P \rightarrow a^6S$ assignment. Therefore, a definitive assignment of the 620 nm feature in Xe was not achieved in Paper II with excitation of the z^6P state.

The emission spectroscopy produced with red site $z^6P \leftarrow a^6S$ excitation in solid Ar and Kr led to the assignment of the bands located at 590 and 585.7 nm , respectively, to the $a^6D_{9/2} \rightarrow a^6S_{5/2}$ transition of atomic Mn. However, this also presents an inconsistency, because although the emission features show a clear asymmetry and a small matrix shift from the gas phase position, the 585.7 nm feature in Kr is blue of the same assigned feature in Ar. In the case of the blue site emissions at 625 and 626 nm in Ar and Kr, respectively, the broad spectral widths and long temporal decays are in conflict, leading to only tentative a^6D state assignments of these bands. Analysis of the luminescence spectroscopy resulting from direct photoexcitation of the $a^6D_J \leftarrow a^6S$ transition of atomic Mn can therefore provide straightforward emission assignments and greater insights into the processes leading to their production. In addition, excitation spectra recorded for the $a^6D \leftarrow a^6S$ and $z^6P \leftarrow a^6S$ transitions allow a critical analysis of the $P \leftarrow S$ and $D \leftarrow S$ absorption processes of matrix-isolated metal atoms. These analyses provide further

insight into the interaction between the guest metal atom and the solid rare gas host. The 6D state data allow a further differentiation between the red and blue sites already studied with z^6P and z^8P state excitation in Papers I and II.

The present paper is structured as follows: First, the 6D state excitation spectroscopy recorded monitoring the emission features in the red spectral region are presented individually for each Mn/RG system. Time-resolved and time-gated emission spectra recorded with pulsed laser excitation of the excitation bands assigned to the $a^6D \leftarrow a^6S$ transition of Mn are then presented. Excited state lifetime measurements of the red emission features are also made and where possible, the radiative decay times are identified. Following an assessment of the sites of isolation, the excitation band profiles are then analyzed with respect to the effect of the excited state interaction within the specific site of isolation.

II. EXPERIMENT

Details of the emission arrangement used in the present work have been given in previous publications^{1,2} from our group. The laser excitation spectra presented in this study were recorded by scanning the direct output of the tunable Quantel TDL-90 dye laser, pumped by the second harmonic of the Quantel YG-980 Nd:YAG laser. Rhodamine 590 was the dye used to cover the spectral range 555 to 585 nm , while Rhodamine 610 was used in the range 572 to 600 nm . The laser excitation spectra presented have not been corrected for the dye curves. Scans are merged in the figures to provide complete coverage for the spectral ranges of interest. It was found that the unfocused output of just the oscillator in the TDL-90 dye laser provided sufficient excitation intensity to produce the red bands with acceptable S/N ratios when photon-counting was used for emission detection. At the maxima of the two dyes used, the laser energy has been measured with a Moletron (EnergyMax, model 500/J9LP) pyroelectric joulemeter as $15 \mu\text{J}/\text{mm}^2$. The spectral resolution of the dye laser is 0.8 cm^{-1} in the wavelength range covered by these two dyes. Time-resolved emission spectra (TRES) were recorded using an Andor Technologies iStar DH720 iCCD (intensified charge coupled device) detector mounted on the SP500i imaging spectrograph. Decay times were measured with the time-correlated single photon counting (TCSPC) technique, as described in Paper II, with a Hamamatsu R928P photon counting photomultiplier tube (PMT) using a 2 GHz multichannel scaler (MCS) (Fast ComTec, Model 7886).

III. RESULTS

The following sections present the excitation spectra recorded using tunable dye laser radiation for the Mn/RG matrix emission in the red spectral region, i.e., in the vicinity of the gas phase³ $a^6D_{5/2} \leftrightarrow a^6S_{5/2}$ transition at 573.03 nm ($17\,451 \text{ cm}^{-1}$). All the spectra shown were recorded in annealed Mn/RG samples that were prepared under conditions chosen for optimal isolation of atomic manganese. Full details of the sample preparation and annealing procedures are given in Ref. 7.

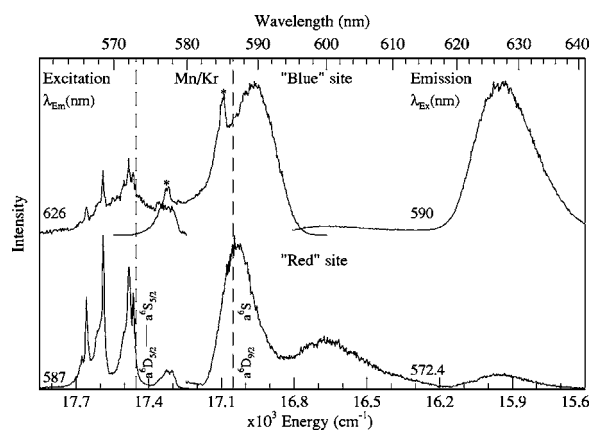


FIG. 2. Laser excitation spectra recorded at 12 K in a Mn/Kr sample annealed to 34 K, in the vicinity of the gas phase $a^6D \leftrightarrow a^6S$ transition (dashed vertical line on the left) monitoring the blue and red site emission features present at 626 and 587 nm, respectively. A comparison of the emission produced with red site a^6D excitation at 572 nm is made on the right, with that produced with blue site excitation at 590 nm. The excitation spectra shown on the extreme left were both recorded with Rhodamine 590, the scan shown in the middle trace in the upper panel was recorded with Rhodamine 610.

A. Mn(a^6D)/Kr

The three red emission bands produced in Mn/Kr samples with “red” site (400 nm) excitation of the atomic Mn $z^6P \leftarrow a^6S$ transition are, as presented in Paper II, located at 587, 604 and 626 nm. The emission features centered at 626 and 587 nm were tentatively assigned to the metastable $a^6D_{9/2}$ state for Mn atom occupancy in the blue (1°) and red (2°) sites, respectively, in Kr matrices. In addition to these thermally stable emission features, the unstable (3°) site of isolation in Mn/Kr, produces a broad emission band at 604 nm.

The emission spectrum recorded with laser excitation at 572.4 nm is shown in the bottom trace on the right in Fig. 2. The scan shown was recorded for a sample annealed to 34 K and clearly consists of the same three emission features already obtained with z^6P state excitation. It is noteworthy that this emission spectrum closely matches that shown in Fig. 9 (Trace A) of Moskovits’ earlier luminescence work⁸ on Mn/Kr matrices produced with 578 nm dye laser excitation. No excitation spectra were presented in the earlier Mn/Kr study for these emission bands, which were attributed to manganese dimer. This attribution was made on the basis of the presence of Mn_2 in the krypton samples and the assumed absence of pumpable atomic Mn transitions in this spectral region. However, as revealed in the present emission lifetime measurements, the “forbidden” 6D - 6S gas phase transitions are greatly enhanced in the site environments of the solid rare gases, with the result that the atom can be pumped with quite low dye laser powers.

The laser excitation spectrum recorded with Rhodamine 590 (Rh590) for the dominant 587 nm emission band is presented on the bottom left in Fig. 2. Indicated by the dashed vertical line is the position of the $a^6D_{5/2} \leftarrow a^6S_{5/2}$ gas phase transition. Inspection of the recorded excitation spectrum, reveals four sharp features each showing additional resolved components. Excitation recorded with Rh590, monitoring the

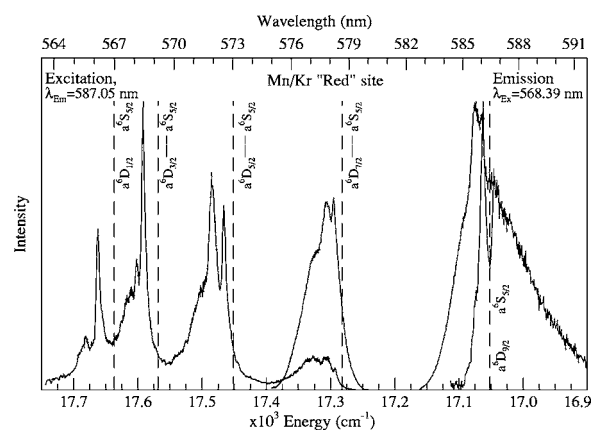


FIG. 3. High resolution laser excitation spectra recorded at 12.5 K in an annealed Mn/Kr sample. The spectra were recorded with Rhodamine 590 monitoring emission at 585.7 nm and with Rhodamine 610 monitoring emission and 587 nm. The dashed vertical lines indicate the positions of the five gas phase (Ref. 3) $a^6D_J \leftrightarrow a^6S$ transitions to the excited spin-orbit levels of the a^6D_J state. The emission spectrum shown on the right was recorded with excitation of the $J=3/2$ spin-orbit level at 568.39 nm. It is evident that all features including the emission, are slightly blue of the gas phase transitions (Ref. 3), indicating a small matrix shift on the $a^6D \leftrightarrow a^6S$ transitions. Particularly noteworthy is the overlap of the excitation and emission scans at 585.7 nm recorded for the $J=9/2$ level.

626 nm emission, was much weaker and, as shown in the upper left trace of Fig. 2, reveals the same structured bands but also contains a broad, red-shifted underlying feature. When this excitation scan was extended to the longer wavelengths with Rhodamine 610 (Rh610), a strong broad band centered at 590 nm was obtained, as shown in the middle of the upper panel of Fig. 2. This band is featureless except for the two narrow lines indicated by the asterisks.

To examine the origin of the multiple features in the excitation spectrum recorded for the red site 587 nm emission, the laser was scanned slower and the resulting higher resolution (more data points) spectrum is shown on the left in Fig. 3. The laser excitation scan was also extended to the red using the dye Rh610, the results of which are shown in the center right of Fig. 3. Very sharp lines are clearly present on each of the five main features in the excitation spectrum recorded with the two dyes. The lowest energy lines in the five resolved features are located at 566.18, 568.44, 572.54, 578.27 and 585.75 nm. The composite high resolution scan done in the complete wavelength range, shown in Fig. 3, contains the two sharp features indicated by asterisks in Fig. 2, at 578 and 585 nm in the excitation scan of the blue site 626 nm emission. These two features are clearly the two lowest energy excitation transitions of the red site.

A comparison is made in Fig. 3, of the excitation spectrum recorded monitoring the 587 nm emission and the five transitions arising from the electric-quadrupole⁹ selection rules ($\Delta S=0$, $\Delta L=\pm 2$ and $\Delta J=0, \pm 1, \pm 2$), between the ground $a^6S_{5/2}$ state and spin-orbit levels of the a^6D_J state of atomic Mn ($J=1/2, 3/2, 5/2, 7/2$ and $9/2$). The very close match between the matrix features and the gas phase transitions is evident in this figure. The extent of the closeness is revealed in Table I by the comparison of the splitting observed for the lowest energy resolved excitation features (70, 126, 173 and 221 cm^{-1}) with the splitting (69, 116, 170

TABLE I. Details of the resolved excitation features recorded monitoring the red site emission bands in the red spectral region for the Mn/Ar, Mn/Kr and Mn/Xe matrix systems. Spectral positions of the observed excitation features and the gas phase energies for the individual $a^6D_J \leftrightarrow a^6S_{5/2}$ transitions are indicated in nanometer (nm) and wave number (cm^{-1}) units for the individual spin-orbit levels. Δ_{GP} indicates the splitting between successive spin-orbit levels in the gas phase³ (GP) and Δ_{RG} is the splitting recorded for the three RG matrix systems. The shifts (δ) of the observed matrix bands are presented in wave number units.

Mn gas phase		Mn/Ar excitation			Mn/Kr excitation			Mn/Xe excitation		
Transition (nm/ cm^{-1})	Δ_{GP} (cm^{-1})	Position (nm/ cm^{-1})	Δ_{Ar} (cm^{-1})	δ (cm^{-1})	Position (nm/ cm^{-1})	Δ_{Kr} (cm^{-1})	δ (cm^{-1})	Position (nm/ cm^{-1})	Δ_{Xe} (cm^{-1})	δ (cm^{-1})
$a^6D_{1/2} \leftrightarrow a^6S_{5/2}$ 566.98/17637	69	568.0/ 17605	61	-32	566.18/ 17662	70	+25	565.0/ 17699	69	+62
$a^6D_{3/2} \leftrightarrow a^6S_{5/2}$ 569.21/17568	116	570.0/ 17544	107	-24	568.44/ 17592	126	+24	567.2/ 17630	117	+62
$a^6D_{5/2} \leftrightarrow a^6S_{5/2}$ 573.03/17452	170	573.5/ 17437	184	-15	572.54/ 17466	173	+14	571.0/ 17513	176	+61
$a^6D_{7/2} \leftrightarrow a^6S_{5/2}$ 578.63/17282	230	579.6/ 17253	223	-29	578.27/ 17293	221	+11	576.8/ 17337	231	+55
$a^6D_{9/2} \leftrightarrow a^6S_{5/2}$ 586.43/17052		587.2/ 17030		-22	585.75/ 17072		+20	584.6/ 17106		+54

and 230 cm^{-1}) between the spin-orbit levels in the gas phase. On the basis of the close match between the matrix and the gas phase excitation spectroscopy, the narrow lines in Kr are assigned to $a^6D_J \leftrightarrow a^6S_{5/2}$ transitions. Thus, the five lines expected for the electric-quadrupole $a^6D_{(J=9/2-1/2)} \leftrightarrow a^6S_{5/2}$ transition have been identified in Mn/Kr matrices.

The excitation transitions observed in solid Kr occur, as given by δ in Table I, to higher energy than the gas phase positions³ by approximately 20 cm^{-1} . Since the gas phase spin-orbit splittings (Δ_{GP}) in the excited a^6D state are maintained in Kr matrices, the blue-shift is attributed to a weak stabilization of the ground $3d^5 4s^2 a^6S_{5/2}$ state of atomic Mn isolated in the red (2°) site.

1. Red site—585.7 nm emission

A high resolution scan of the 587 nm emission band is presented on the extreme right in Fig. 3. When this band is recorded under low resolution (as shown in Fig. 2), it is centered at 587 nm but the high resolution scan shown in Fig. 3 reveals the existence of a sharp emission feature at 585.75 nm (17 072 cm^{-1}) and a red wing that extends past 591 nm. As observed in the laser excitation lines, the narrow emission line is also slightly (+20 cm^{-1}) to the blue of the gas phase $a^6D_{9/2} \leftrightarrow a^6S_{5/2}$ transition at 586.43 nm (17 052 cm^{-1}).³ At temperatures in excess of 15 K the intensity of the sharp feature is reduced relative to the red wing, and at still higher values, the sharp feature has nearly been completely removed. This temperature dependence (not shown) was completely reversible, and indicates that the 17 072 cm^{-1} feature is the zero-phonon line in the electronic $a^6D_{9/2} \rightarrow a^6S_{5/2}$ transition. It is also clear in this figure that the excitation and emission band maxima coincide. Thus, the emission of the $J=9/2$ level of atomic manganese does not exhibit a Stokes shift when isolated in the red site of Kr.

A comparison of the emission produced with $J=7/2$ and $J=9/2$ excitation is made on the left panel in Fig. 4. It is clear in the figure that the band obtained with $J=9/2$ excitation at 585 nm is identical to that obtained with $J=7/2$ excitation at 578 nm, once the laser scatter has been removed from the former. Excitation of the three other J levels in the a^6D state also produce emission centered at 585.7 nm, which is assigned to the lowest energy spin-orbit level of $a^6D_{9/2}$ state atomic Mn. Shown in the right panel of Fig. 4 are the decay curves recorded for the 585.7 nm emission with excitation into the five spin-orbit levels of the a^6D state. Here also the decay curves are identical, indicating that in the Kr

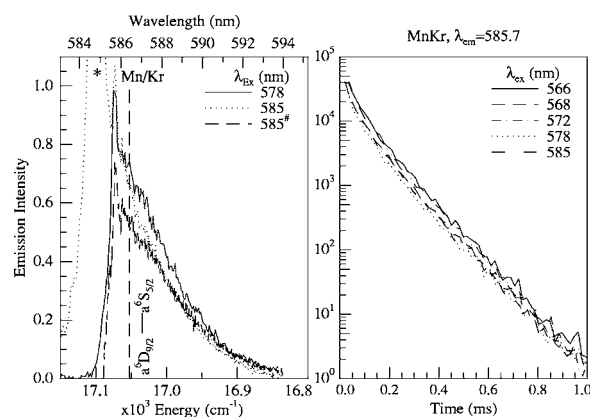


FIG. 4. High-resolution scans of the 585.7 nm Mn/Kr emission produced with laser excitation at 578 and 585 nm corresponding to the $a^6D_{7/2} \leftrightarrow a^6S_{5/2}$ and $a^6D_{9/2} \leftrightarrow a^6S_{5/2}$ transitions, respectively. Once the laser scatter (shown by the asterisk) is removed from the scan recorded with 585 nm excitation, it is clear that the subtracted emission (shown by the hash symbol) produced with 9/2 excitation is identical to that produced with 7/2 excitation. The vertical line indicates the position of the gas phase $a^6D_{9/2} \leftrightarrow a^6S_{5/2}$ transition. The panel on the right-hand side shows a comparison of the 585.7 nm emission decay curves recorded with excitation into the five spin-orbit levels of the a^6D state. All the decay curves are identical and long-lived, extending up to 1 ms.

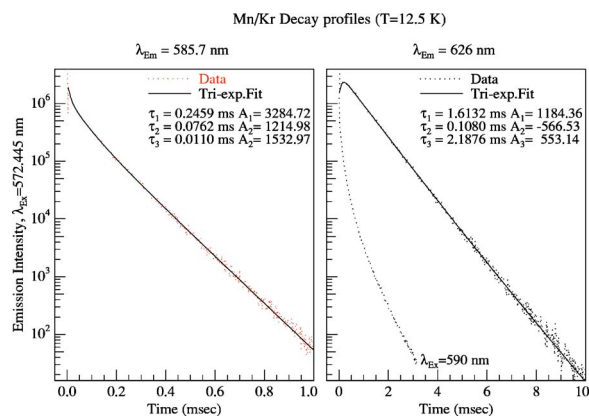


FIG. 5. Shown on the left is the decay profile of the Mn/Kr 585.7 nm emission feature recorded at 12 K using TCSPC following pulsed laser excitation at 572.4 nm. The parameters extracted in the triple exponential fit are listed in the plot. The decay curve shown on the right was recorded for the 626 nm emission and produced with the same excitation. The presence of a risetime on this decay is clearly evident in the triple exponential fit conducted. Also shown in this panel is the decay of the 626 nm emission but produced with direct, blue site excitation at 590 nm.

matrix, intra-multiplet relaxation (IMR) between the spin-orbit levels and the emitting $J=9/2$ level occurs at rates much faster than the radiative decay. However, as will be shown now, the decay rates of these forbidden transitions are relatively slow, $\sim 10^3 \text{ s}^{-1}$, which means the IMR rates must only be an order of magnitude in excess of this value, to produce identical emission bands and decay kinetics.

Excited state lifetimes were measured with the photon counting PMT and a fast multichannel scaler. The left-hand panel in Fig. 5 presents the decay profile recorded at 12.5 K for the 585.7 nm emission feature produced with excitation into the resolved $J=7/2$ feature. A successful fit of the decay profile was achieved with a triple exponential function, yielding decay components with lifetimes of 246, 76 and 11 μs . The longest component dominated the decay profile recorded at 12.5 K. Recording the decay profile of the 585.7 nm emission at higher temperatures showed that the true radiative lifetime for the $a^6D_{9/2} \rightarrow a^6S_{5/2}$ transition had not been observed at 12.5 K as all components were shorter at 14.0 K. Therefore, the dominant 246 μs decay component at 12.5 K is identified in Table II as the observed lifetime of the 585.7 nm emission in Mn/Kr.

2. Blue site—626 nm emission

Resolved a^6D state features are also present in the excitation spectra, shown in the upper left of Fig. 2, recorded monitoring the blue site emission centered at 626 nm. However, the main excitation feature recorded for the 626 nm emission is featureless and centered at 590 nm. As shown in Fig. 2, direct excitation of the a^6D state with Rh590 produces mostly the red site 585.7 nm emission features, but also a small amount of the blue site 626 nm band. The occurrence of emission bands for both sites¹⁰ arises, as shown in Fig. 2, because of the spectral overlap present in their recorded a^6D state excitation spectra. In contrast, the excitation spectra recorded in Paper I for the red and blue sites on the $z^6P \leftarrow a^6S$ transition were shifted by approximately

TABLE II. Photophysical characteristics and excited state assignments of the red site emission features produced with direct excitation of the $3d^64s^6D_J \leftarrow 3d^54s^2a^6S_{5/2}$ transitions of matrix-isolated atomic manganese in solid Ar and Kr. λ_{Em} indicates the emission band center in nm and wavenumber units. The matrix shift from the gas phase (Ref. 3) $a^6D_{9/2} \leftrightarrow a^6S_{5/2}$ transition at 586.43 nm ($17\,052 \text{ cm}^{-1}$) is indicated in wavenumber (cm^{-1}) units by δ . The 620 nm emission in Xe is presented with the blue site data of Ar and Kr in Table III. The dominant decay components are shown in bold font.

System	λ_{Em} (nm)/(cm^{-1})	δ (cm^{-1})	Decay times (μsec)
Mn/Ar	590.0/16949	-103	1167
			442
			83
Mn/Kr	585.75/17072	+20	246
			76
			11
Mn/Xe	Not observed	—	—

800 cm^{-1} and thereby well resolved. More importantly, the resolved spin-orbit structure present on the red site excitation spectra (recorded for the 585.7 nm emission) is absent on the featureless, broad band located at 590 nm recorded for the blue site emission at 626 nm. Furthermore, the blue site emission exhibits a Stokes' shift of 975 cm^{-1} as listed in Table III. This contrasts with the red site where the Stokes' shift does not exist, i.e., the zero phonon line has been observed in both excitation and emission.

Time-resolved emission spectra (TRES) were recorded with iCCD camera detection for the 626 nm and 585.7 nm emission bands and pulsed laser excitation of the feature assigned to the $a^6D_{5/2} \leftarrow a^6S_{5/2}$ transition. Although not presented, the 585.7 nm feature assigned to the $a^6D_{9/2}$ state was observed in the TRES to decay on a μs time scale. This is consistent with the TCSPC measurements presented on the left in Fig. 5, in which the observed lifetime of the $a^6D_{9/2}$ state is identified as 246 μs . In contrast, the intensity of the 626 nm emission feature was observed in the TRES to still be increasing on this time scale.

The temporal characteristics of the 626 nm emission feature recorded with TCSPC are shown on the right in Fig. 5. Inspection of the decay profile recorded with 572 nm excita-

TABLE III. Photophysical characteristics of the blue site luminescence in Ar, Kr and Xe matrices. The excitation and emission maxima are quoted in wavelength (nm) and wavenumber (cm^{-1}) units. The Stokes shifts measured in the three matrices are listed as δ in wavenumber (cm^{-1}) units. All the emission bands listed are assigned to the a^6D state. The dominant decay components are shown in bold font.

Mn/RG	λ_{Ex} (nm)/(cm^{-1})	λ_{Em} (nm)/(cm^{-1})	δ (cm^{-1})	Decay times (μsec)
Ar	586/17065	625/16000	1065	1007
				369
Kr	590/16949	626/15974	975	1252
				397
				119
Xe	590/16949	620/16129	820	1663
				683
				211

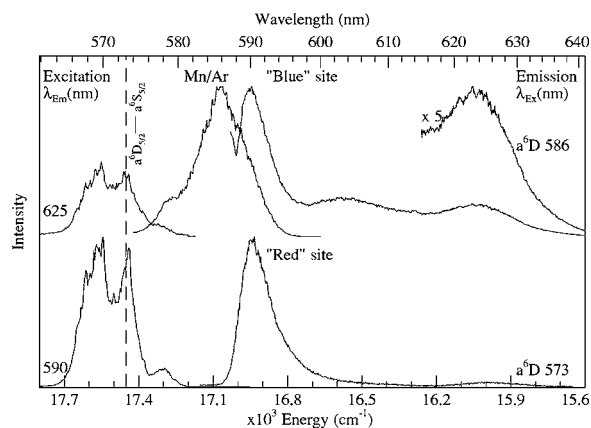


FIG. 6. Mn/Ar laser excitation spectra recorded at 12.5 K, in the vicinity of the $a^6D_{5/2} \leftrightarrow a^6S_{5/2}$ gas phase transition monitoring the red site and blue site emission features at 590 and 625 nm, respectively. The sample was deposited at 12.5 K and annealed to 29 K.

tion reveals a rising portion at short time corresponding to a slow feeding step in the production of the 626 nm feature. This is the same behavior detected in the TRES described above. A triple exponential function was required to provide an adequate fit of the 626 nm emission decay profile, yielding two decay times 2.19 and 1.61 ms and a rising component of 108 μ s. The decay profile recorded for the 626 nm emission produced with direct 590 nm excitation is also shown in the panel on the right-hand side of Fig. 5. Complex kinetics are once again exhibited, with a triple exponential required but this time, a risetime is not present. The dominant decay component had a lifetime of 119 μ s, the two other components in order of importance had, as listed in Table III, values of 397 μ s and 1.252 ms, respectively. The 626 nm emission decay profile was also recorded at 14.0 K and found to be sensitive to temperature in this small 12–14 K range. Hence, the radiative lifetime for the 626 nm feature has not been measured at 12 K.

B. Mn(a^6D)/Ar

The luminescence of atomic Mn isolated in solid Ar produced with z^6P state excitation exhibits three site specific emission features at 590, 625 and 604 nm corresponding to the 1° red, 2° blue and 3° site occupancies, respectively. The 590 nm emission feature, resulting from red (1°) site excitation at 393.4 nm, was assigned to the $a^6D_{9/2} \rightarrow a^6S_{5/2}$ transition in Paper II. Blue (2°) site excitation at 380 nm favors the 625 nm band that was only tentatively assigned to broadened a^6D state emission. Careful annealing experiments showed the 604 nm feature arises from atomic Mn occupancy in a thermally unstable site in solid Ar. On the right in Fig. 6, the emission produced in Mn/Ar samples with laser excitation at 573 and 586 nm are shown. The same three emission bands are observed with minimal amounts of the 604 nm band since the sample used had been annealed to 29 K.

The left-hand side of Fig. 6 presents the laser excitation spectra recorded in the vicinity of the $a^6D_{5/2} \leftrightarrow a^6S_{5/2}$ gas phase transition³ for the two thermally stable site emissions previously observed with z^6P state excitation. Inspection of the excitation scans recorded with Rh590 by monitoring the

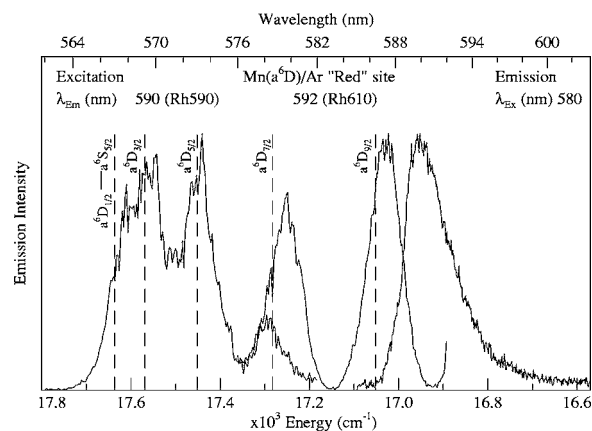


FIG. 7. Laser excitation spectra recorded for Mn/Ar at 12 K, with Rhodamine 590 and Rhodamine 610 monitoring emission at 590 and 592 nm, respectively. The dashed vertical lines indicate the gas phase positions of the individual $a^6D_J \leftrightarrow a^6S_{5/2}$ transitions (Ref. 3). Particularly noteworthy is the overlap of the excitation and emission scans recorded for the $J=9/2$ level at 588.8 nm which provides an estimate of the zero phonon line for this transition. Also evident is a small red-shift of the entire excitation and emission bands from the gas phase positions.

590 (bottom trace) and 625 nm emission features, reveals structured profiles in the same spectral region. The excitation profile recorded with Rh610, monitoring the 625 nm emission feature, produces a broad band centered at 586 nm exhibiting, as shown in the upper center of Fig. 6, no resolved features but the indication of a shoulder at 578 nm.

An overlay of the excitation spectra recorded monitoring the Mn/Ar “red” site 590 nm emission with the gas phase $a^6D_J \leftrightarrow a^6S_{5/2}$ state transitions is presented in Fig. 7. Shown also in this figure is the excitation scan recorded with Rh610, which reveals the location of the fifth, $J=9/2$ spin-orbit level. Thus the complete excitation scan of the 590 nm emission exhibits five resolved features, located at 568.0, 570.0, 573.5, 579.6 and 587.2 nm. It is evident in this figure that all the matrix transitions are red-shifted from the gas phase by approximately 25 cm^{-1} , but all show similar splitting intervals as in the gas phase. The intervals listed in Table I, between the resolved features in the excitation scan, recorded monitoring the 590 nm emission in solid Ar, allows a definitive assignment of transitions to the individual spin-orbit levels of the excited a^6D state.

The right-hand side of Fig. 7 presents a high-resolution emission spectrum produced with excitation at 580 nm, close to the band maximum of the $J=7/2$ level in Ar at 579.6 nm. The resulting broad emission feature is centered at 590 nm and exhibits a linewidth (FWHM) of 100 cm^{-1} . The overlap evident in Fig. 7, between the excitation and the emission of the $J=9/2$ level, allows an unambiguous assignment of the 590 nm emission in solid Ar to the $a^6D_{9/2} \rightarrow a^6S_{5/2}$ transition. With this assignment, the emission of matrix-isolated atomic Mn is red-shifted from the gas phase position by -103 cm^{-1} . The 590 nm emission band was found, as observed in the Mn/Kr system, to be independent of the J state used for excitation. This indicates that fast IMR also occurs for the a^6D_J states of Mn atoms in Ar lattices. In contrast to the Mn/Kr system, the band shape did not show any significant dependence on temperature, indicating that resolved

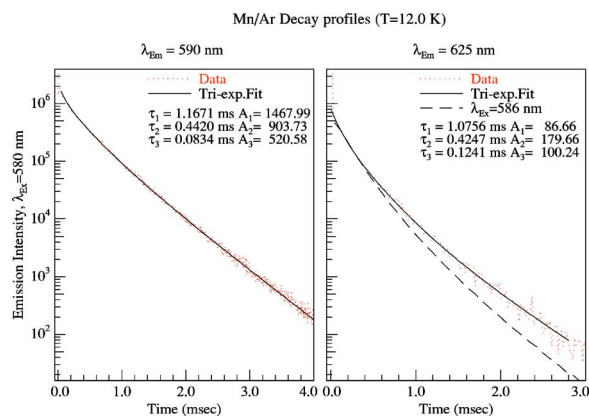


FIG. 8. Shown on the left is the decay profile of the Mn/Ar 590 nm emission feature recorded at 12 K using TCSPC following pulsed laser excitation at 580 nm, corresponding to $J=7/2$ excitation. The parameters extracted in the triple exponential fit are listed in the plot. The decay curve shown on the right was recorded for the 625 nm emission and produced with the same excitation. The triple exponential fit conducted is also shown. Also shown on the right (with the dashed line) is the decay of the 625 nm emission but produced with direct blue site excitation at 586 nm.

phonon structure is not present on the 590 nm emission band in Ar. However, due to the approximate mirror-image of the excitation and the emission bands, the location of the zero phonon line (ZPL) can be estimated from the point of overlap of the two bands. This occurs, as shown in Fig. 7, at 588.8 nm yielding a ZPL at $16\,984\text{ cm}^{-1}$ and corresponds to a shift of -68 cm^{-1} for the pure electronic $a^6D_{9/2} \rightarrow a^6S_{5/2}$ transition of atomic manganese in solid Ar. The value compares favorably with the estimate of $17\,020\text{ cm}^{-1}$ for the ZPL (band origin) obtained from a lineshape analysis of this emission band in Paper II.

Excited state decay profiles recorded for the 590 nm emission indicate complex kinetics even for direct $a^6D \leftarrow a^6S$ excitation. Figure 8 presents a decay profile recorded monitoring the 590 nm emission feature produced with pulsed laser excitation at 580 nm. Inspection of the data and the fit, shown on the left, reveals that an adequate fit of the recorded decay profile required the use of a triple exponential function. The largest contribution to the decay curve has a lifetime of 1.167 ms at 12 K. The additional components extracted have, as listed in Table II, lifetimes of 442 and 83 μs , and all have substantial amplitudes. The observed lifetime of the 590 nm feature, assigned to the $a^6D_{9/2} \rightarrow a^6S_{5/2}$ transition, is identified as 1.17 ms at 12 K. Decay profiles recorded at 25 K (not shown) differ from that shown on the left in Fig. 8. Therefore, the radiative lifetime of the transition has not been observed at the lowest temperature attainable (12 K) in the present experiment.

The bottom trace on the right in Fig. 6 presents a summary of the luminescence spectroscopy recorded with excitation of the a^6D state of atomic Mn isolated in solid argon. The weak emission feature at 625 nm was tentatively assigned in Paper II to emission of the a^6D state Mn atom isolated in the blue site of Ar. The a^6D state excitation spectra recorded for the two thermally stable 590 and 625 nm emissions, presented on the left in Fig. 6, exhibit distinct spectral shifts, as previously observed in the z^6P state excitation spectra, and show very different linewidths. Thus, as

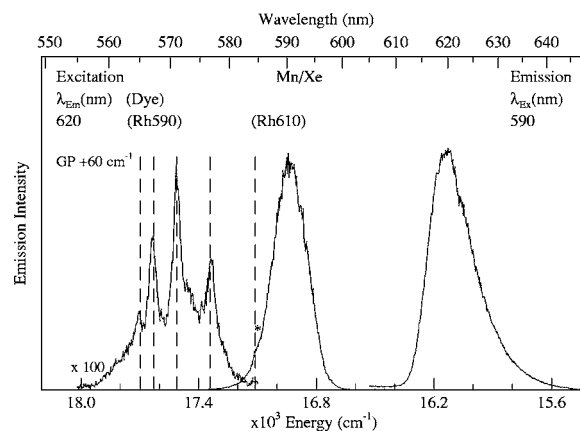


FIG. 9. Laser excitation spectra recorded in Mn/Xe at 12 K, with Rhodamine 590 and Rhodamine 610 monitoring emission at 620 nm. The dashed vertical lines indicate the gas phase positions of the individual $a^6D_J \leftrightarrow a^6S_{5/2}$ transitions (Ref. 3) shifted by $+60\text{ cm}^{-1}$. The broad spectral shapes of the excitation (590 nm) and emission (620 nm) bands contrast with the narrow structured bands recorded with Rh590. The presence of the latter bands is interpreted as the first indication of the existence of red site occupancy of Mn atoms in Xe matrices. However, the emission of this site was not detected in the present study.

shown on the upper left in Fig. 6, the blue site emission at 625 nm has a broad excitation band centered at 586 nm. In contrast, the excitation spectrum of the red site emission at 590 nm exhibits resolved spin-orbit transitions. A fit of the decay profile recorded for the 625 nm emission, shown on the right in Fig. 8 using a triple exponential function, yielded excited state lifetime components of 1.075 ms, 425 and 124 μs . Although all the components show comparable amplitudes, the 425 μs component dominates the excited state decay profile recorded at 12.0 K.

The temporal decay of the Mn/Ar blue site emission at 625 nm, when produced with direct 586 nm excitation, is shown by the dashed line in the panel on the right in Fig. 8. The decay curve is quite similar to that produced with 580 nm excitation. The major difference between the two curves is, as listed in Table III, the greater dominance of the 0.4 ms component when the emission is produced with 586 nm excitation. Accordingly, the observed excited state lifetime of the blue site 625 nm emission in Ar is identified as 0.4 ms.

C. Mn(a^6D)/Xe

Figure 9 presents the laser excitation spectra recorded for Mn/Xe in the vicinity of the gas phase $a^6D_J \leftrightarrow a^6S_{5/2}$ transitions of atomic manganese, monitoring the 620 nm emission previously observed with z^6P excitation and presented in Paper II. The two excitation scans shown on the left in Fig. 9 have not been corrected for the wavelength response of the dyes used, Rhodamine 590 and 610. Inspection of Fig. 9 reveals four resolved excitation features at 565.0, 567.2, 571.0 and 576.8 nm recorded with Rh590. The scan obtained with Rh610 reveals two features—the broad band centered at 590 nm and a weak shoulder close to 585 nm. Both excitation scans were recorded monitoring the 620 nm emission. For the purposes of analysis, the locations of all five $a^6D_J \leftrightarrow a^6S_{5/2}$ transitions of atomic manganese are

shown in Fig. 9 shifted by $+60\text{ cm}^{-1}$ from their positions in the gas phase. The comparison of the observed Xe matrix band positions with the gas phase transitions from the ground $a^6S_{5/2}$ state to the individual a^6D_J states, indicates an identical splitting pattern³ for the spin-orbit levels $J=7/2, 5/2, 3/2$ and $1/2$. Thus the splittings between the observed excitation bands are 69, 117 and 176 cm^{-1} , as listed in Table I, while the gas phase splittings between the spin-orbit levels of the a^6D_J state are 69, 116, and 170 cm^{-1} for the $1/2 \leftrightarrow 3/2$; $3/2 \leftrightarrow 5/2$ and $5/2 \leftrightarrow 7/2$ intervals, respectively. The favorable comparison between the shifted gas phase lines and the observed shoulder at 584.6 nm in the Rh610 excitation scan, shown by the asterisk in Fig. 9, allows its assignment to the missing $J=9/2$ spin-orbit level.

A conspicuous feature of the excitation band recorded with Rh610 (shown in the middle of Fig. 9) centered at 590 nm is the large linewidth. It is much greater than the higher energy spin-orbit levels recorded with Rh590, but closely matches the bandwidth of the 620 nm emission. The observation of blue-shifted excitation band profiles for the five resolved spin-orbit levels ($J=1/2, 3/2, 5/2, 7/2$ and $9/2$) and a red-shift on the main 590 nm excitation band is also rather striking in Fig. 9. From similar observations in the Mn/Ar and Mn/Kr systems, this behavior indicates that two distinct matrix environments produce the structured and featureless excitation bands recorded in MnXe with Rh590 and Rh610, respectively. In the Mn/Ar and Mn/Kr systems, it will be remembered that the red and blue sites of isolation have very different linewidths. Thus, in the blue site, the broad excitation linewidth matches that of the emission band, while the red site has narrow, resolved spin-orbit lines in excitation and unshifted emission. A careful search was made for the emission of the red site atoms in Xe with Rh590 excitation of the resolved J states, but without success. This is not entirely understood, but it is suspected that it is related to the very small amounts of this site that exists in Mn/Xe. It should be noted that the red site in Mn/Xe was not detected on any of the other excited states of atomic Mn studied and must be present in very small amounts. The narrow linewidth of the a^6D state spin-orbit levels aids in their detection with laser excitation, but a weak, slightly broadened red site emission will not be detected as easily. The reason for the poor definition of the red site $J=9/2$ excitation feature is due to its weakness and location, i.e., it overlaps the high energy side of the much more intense, blue site excitation band centered at 590 nm .

The highest energy $a^6D_J \leftarrow a^6S_{5/2}$ transitions observed in solid Xe, exhibit an average blue matrix shift (δ) of approximately $+60\text{ cm}^{-1}$, see Table I. The observation that the gas phase splittings between the individual spin-orbit states are maintained in the solid infers that the observed matrix shift arises as a result of stabilization of the $a^6S_{5/2}$ ground state within this site of isolation in solid Xe.

An adequate fit of the decay profile recorded monitoring the Mn/Xe 620 nm feature was achieved using a triple exponential function as shown by the analysis presented on the left in Fig. 10. The extracted decay components have values of 1.663 ms, 683 and $211\text{ }\mu\text{s}$. Inspection of the relative amplitudes of the decay components in Fig. 10 reveals that the

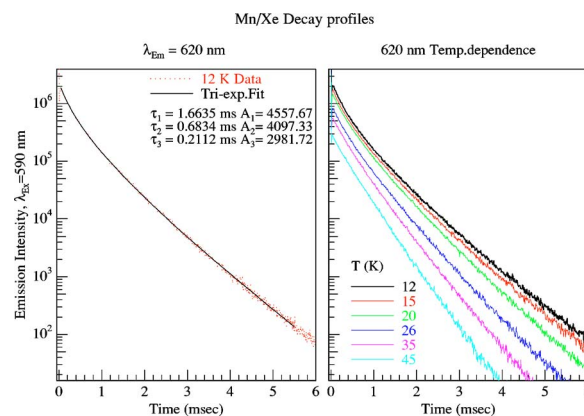


FIG. 10. Shown on the left is the decay profile of the Mn/Xe 620 nm emission feature recorded at 12 K using TCSPC following pulsed laser excitation at 590 nm . The parameters extracted in the triple exponential fit are listed in the plot. The decay curves shown on the right were recorded for the 620 nm emission at the specified temperatures.

1.663 ms decay component dominates at 12.5 K . However, the substantial amplitudes extracted for the other components indicates their significance. Recording emission decay profiles at temperatures in excess of 12.5 K revealed only small differences in the decay characteristics. The decay curves recorded at elevated temperatures are presented on the right in Fig. 10. These values reinforce the assignment of the 620 nm emission to the a^6D state.

IV. DISCUSSION

A. Mn(a^6D)/RG luminescence

The presence in Fig. 2 of excitation bands in the region of the $a^6D_J \leftarrow a^6S_{5/2}$ transitions, indicates that the a^6D state is indeed responsible for all three red emission features in Mn/Kr matrices, because as shown in Fig. 1, this is the only state of atomic Mn in the $17\,000\text{ cm}^{-1}$ energy region. As observed for the z^6P state, the excitation scans shown in Fig. 2 demonstrate that the a^6D state excitation profiles recorded for the blue and red sites differ considerably. For the present $D \leftarrow S$ excitation scans, the spectral positions are not so strongly dependent on the site of isolation, but the transition lineshapes differ greatly. As is evident on the left-hand side of Fig. 2, the excitation scans vary from highly structured narrow lines, recorded for the red site 587 nm band, to a broad featureless band, recorded for the blue site 626 nm emission.

In the next section, the observed luminescence spectroscopy of the $a^6D_J \leftrightarrow a^6S_{5/2}$ transition of atomic Mn isolated in solid Ar, Kr and Xe is summarized and the trends evident in the recorded excitation and emission spectra are highlighted. Tables II and III collect the photophysical characteristics of the red and blue emission features produced with direct a^6D state excitation of Mn atoms in the solid rare gases Ar, Kr and Xe. Figures 11 and 12 present summaries of the excitation and emission spectra recorded for the a^6D state of atomic Mn isolated in the red and blue sites, respectively.

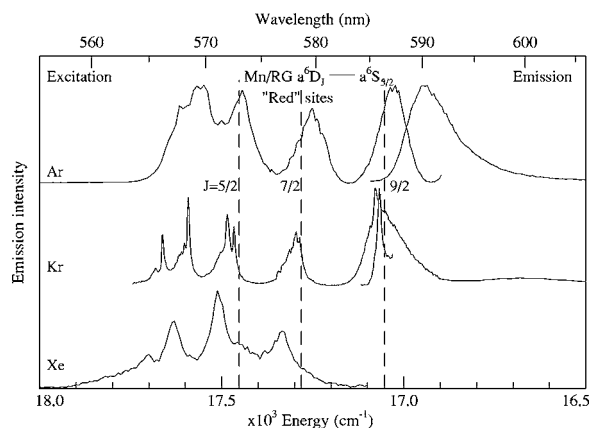


FIG. 11. A comparison of the red site excitation and emission spectra recorded in Ar, Kr and Xe matrices. The correspondence of the ZPLs in the Mn/Kr system is evident as is the small Stokes shift in Mn/Ar. The red site emission was not detected in the Mn/Xe system. The excitation spectra shown were recorded with both Rhodamine 590 and 610.

B. Red site spectroscopy

The excitation spectra recorded in solid Ar, Kr and Xe, monitoring the red emission features tentatively assigned in Paper II to the $a^6D_{9/2} \rightarrow a^6S_{5/2}$ transition of atomic Mn isolated in the “red” site, are compared in Fig. 11. The excitation spectra recorded for this site exhibit resolved features that are assigned, from the splitting intervals and spectral locations, to transitions from the ground $a^6S_{5/2}$ state of atomic Mn to the individual spin-orbit levels of the a^6D state. The spectral locations and assignments of the resolved features for the Mn/Ar, Mn/Kr and Mn/Xe systems are collected in Table I.

The observation in Fig. 11 of the individual spin-orbit levels in excitation is attributed to weak coupling of the a^6D excited state Mn atom to the matrix environment provided by the site of isolation. This is consistent with the small spectral shifts on the recorded excitation features. The matrix-shifts evident on the left hand side of Fig. 11 are identified as -25 , $+20$ and $+60$ cm^{-1} in Ar, Kr and Xe, respectively. Shifts of this small magnitude indicate the Mn atom $a^6D \leftarrow a^6S$ transition energy is rather insensitive in this site of isolation compared with the $z^6P \leftarrow a^6S$ transition examined previously^{1,2} in the solid rare gases.

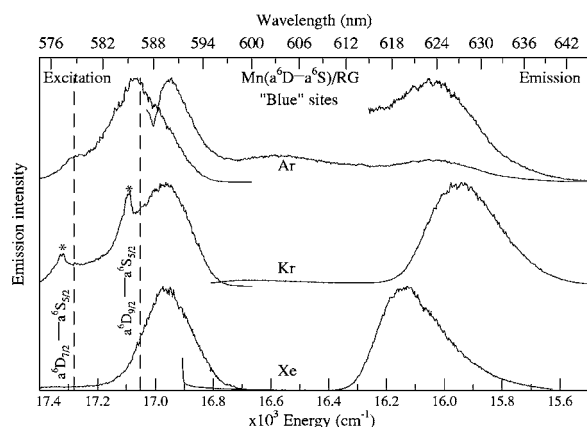


FIG. 12. A comparison of the blue site excitation and emission spectra recorded in Ar, Kr and Xe matrices. All the excitation spectra were recorded with Rhodamine 610.

A progressive matrix-shift to higher energy is observed for the $a^6D \leftarrow a^6S$ excitation spectra recorded from Ar to Xe. As the splittings between the observed bands (assigned to the distinct spin-orbit levels) is maintained in the solid, the unusual blue matrix shift of Xe relative to Ar must be ascribed to the extent of ground state stabilization for the Mn atom present in a given site of isolation within a particular host solid. It thereby indicates the excited 6D state is not interacting as strongly with the host as the ground a^6S state. The comparison of the high-resolution Mn/Kr excitation spectra to the gas phase transitions allowed the assignment of the ZPLs for the $a^6D_{9/2} \leftarrow a^6S_{5/2}$ transition for the Mn/Kr system. The excitation bands in Ar and in Xe are significantly broader than in Kr and do not exhibit resolved phonon structure.

C. Blue site spectroscopy

A comparison of the “blue” site luminescence (excitation and emission) spectroscopy recorded in Mn/Ar, Mn/Kr and Mn/Xe is made in Fig. 12. As observed with the blue site z^6P state excitation bands, the linewidths of the corresponding a^6D state bands are large but the locations are irregular, with Kr and Xe quite similar (both at 590 nm) and Ar to the blue of this at 586 nm. Irregular behavior is also exhibited in the blue site emission spectra, where Xe is the highest energy emitter (620 nm) with Kr the lowest (626 nm) and Ar intermediate (625 nm).

The blue sites in all three matrices exhibit large Stokes shifted emission. The values listed in Table III range from 820 cm^{-1} for Xe to 1056 cm^{-1} for Ar, with Kr intermediate at 975 cm^{-1} . This contrasts strongly with the red site in Kr which exhibits no Stokes shift for the $J=9/2$ emission. The red site in Ar has overlapped excitation and emission with a small Stokes shift of 95 cm^{-1} . As noted earlier, the red site emission in Xe was not detected in the present study.

The lack of structure on the excitation bands of the blue sites and the resolved spin-orbit structure on the red sites is the most striking difference between the two thermally stable sites in the rare gases. This behavior indicates a much stronger interaction of the Mn atom with its solid state environment when isolated in the blue site than in the red site. In turn, this suggests that the atomic spin-orbit coupling is “washed” out by the interaction of the atom and its environment in the blue site. If this is the case, then the spin-orbit designation of the emission may not be appropriate, for the blue sites emission, which will simply be denoted as a^6D without a specified J value.

D. Emission

The emission spectroscopy reported in the previous sections following excitation of the $3d^4s^2 a^6D_1 \leftrightarrow 3d^5 4s^2 a^6S$ transitions is summarized on the right in Figs. 11 and 12. The transition assignments and photophysical properties of the observed emission features are presented in Tables II and III for the red and blue sites, respectively. The most definitive assignment is achieved for the 585.7 nm band in the Mn/Kr system, in which the observed temperature dependence in the emission lineshape allowed the identification of the zero

phonon line (ZPL) for the $a^6D_{9/2} \rightarrow a^6S_{5/2}$ transition at 585.75 nm ($17\,072\text{ cm}^{-1}$). This emission line is blue shifted from the gas phase position³ by only $+20\text{ cm}^{-1}$ —a value that agrees well with the shift exhibited by the $a^6D_J (J = 1/2, 3/2, 5/2, 7/2 \text{ and } 9/2) \leftarrow a^6S_{5/2}$ excitation transitions. Analysis of the excitation spectrum (presented on the upper left of Fig. 2) recorded monitoring the 626 nm band, allows assignment of this emission to the $a^6D \rightarrow a^6S$ transition.

The emission features assigned to the $a^6D_{9/2} \rightarrow a^6S_{5/2}$ transition of Mn atoms isolated in solid Ar, Kr and Xe at 590, 585.75 and 620 nm show uncharacteristic matrix-shifts of -103 , $+20$ and -923 cm^{-1} , respectively. Mn atoms isolated in the red sites of isolation in Ar and Kr (identified in Paper II with z^6P state excitation) lead to the production of the 590 and 585.75 nm features assigned to $a^6D_{9/2}$ state emission. However, the 620 nm feature in Mn/Xe, assigned to the same transition, was identified from the polarizability dependence of its z^6P state excitation spectra to occur from the blue site occupancy. It is suggested that the site size available in the red site of the Kr lattice allows access to the minimum of the excited state potential energy curves, thereby allowing the observation of the ZPL for the $a^6D_{9/2} \rightarrow a^6S_{5/2}$ transition in this site. In solid Ar, the smaller site size does not allow access to the minima of the ground and excited state potentials, causing optical transitions to access steeper, more repulsive final state potentials. This stronger interaction with the host lattice, results in the broadening of the emission lineshapes and the observed red shift on the Ar emission.

In addition to the red site emissions at 590 and 585.7 nm in solid Ar and Kr, respectively, the blue site 625 and 626 nm emission features in these hosts are also assigned as $^6D \rightarrow ^6S$ transitions. These emission bands are produced optimally with a^6D_J excitation at 586 and 590 nm at lower energy than their red site equivalents and correspond to the emission of Mn atoms occupying the blue sites in Ar and Kr. These Stokes shifted emissions are better compared with the 620 nm emission in Mn/Xe, where the Mn atom occupies a site, thought to be a single vacancy. As noted earlier, the J designation of the blue site emission is not given.

V. CONCLUSIONS

Summaries of the matrix excitation and emission spectra recorded in the vicinity of the gas phase $a^6D_{9/2} \leftrightarrow a^6S_{5/2}$ transition are presented in Figs. 11 and 12 for the three rare gases used as hosts in the present study. These spectra demonstrate that the emission features in the red spectral region, tentatively assigned in Paper II to the $a^6D_{9/2} \rightarrow a^6S_{5/2}$ transition in solid Ar, Kr and Xe are indeed produced by metastable $a^6D_{9/2}$ state of atomic Mn. The observation of the individual spin-orbit levels in excitation is attributed to weak coupling between the excited a^6D state Mn atom and the solid-state environment provided by the site of isolation. This contrasts with the excitation spectra recorded monitoring the same emission features, in the vicinity of the gas phase $z^6P_{5/2} \leftrightarrow a^6S_{5/2}$ and $z^8P_{5/2} \leftrightarrow a^6S_{5/2}$ transitions in Paper I, where the excitation spectra showed pronounced Jahn–Teller threefold splitting pattern, characteristic of a strong interaction of the excited electronic state and the host. This com-

parison highlights the stronger interaction of the z^6P and z^8P excited states with the matrix environment than the metastable a^6D state atom.

The conservation of gas phase spin-orbit splittings for the red sites and the featureless blue site excitation spectra, point to a different behavior in these two sites of atomic isolation in the solid matrices. The observed matrix shifts present on the red sites for the the $a^6D_J \leftrightarrow a^6S_{5/2}$ transitions, have been attributed to the extent of ground state stabilization for the isolated Mn atom. The narrow emission produced with direct a^6D_J state excitation allowed the definitive assignment of the 585.7 nm line in the Mn/Kr system to the metastable $a^6D_{9/2}$ state. The Mn/Kr system exhibits a coincidence of the ZPLs in excitation and emission, such that the Stokes shift is nonexistent for the $J=9/2$ level in the a^6D state. In Ar and Xe such definitive assignments are not possible due to the broader excitation/emission spectra recorded. This different behavior is attributed to excited state interactions occurring due to the site of metal atom isolation in the rare gas host. However, the $a^6D_{9/2}$ state is now confidently assigned to the emission features in the red spectral region for these systems.

The multi-exponential decay curves (triple exponentials) recorded for all the emission bands in the Mn/RG systems, even when direct a^6D state excitation is used in annealed samples, indicates that these decay processes are intrinsically complex. This behavior may be connected with the increased excitation linewidths observed for the bands assigned to the larger J spin-orbit levels of the a^6D state. Both effects may result from a removal of the degeneracy of the J values due to weak crystal field splitting¹¹ (CFS) induced in the a^6D state by the rare gas atoms of the lattice. The emission has in all cases been attributed to the $J=9/2$ level, which is subject to CFS producing three distinct levels even in an field of octahedral symmetry, such as that of the single vacancy (substitutional) site in Mn/Xe. This proposal requires detailed lineshape analyses of the recorded a^6D state excitation and emission spectra—work that is currently underway.

ACKNOWLEDGMENTS

This research was funded by the Irish Government *Enterprise Ireland*, SC/98/403 Basic Science research grant to whom M.C. gratefully acknowledges receipt of a Ph.D. studentship. M.R. similarly acknowledges the IRCSET for her Ph.D. studentship. The iCCD used in this work was acquired with the financial support of Science Foundation Ireland, Investigator Grant No. 02/IN.1/B032.

¹M. A. Collier and J. G. McCaffrey, J. Chem. Phys. **122**, 054503 (2005).

²M. A. Collier and J. G. McCaffrey, J. Chem. Phys. **122**, 184507 (2005).

³N.I.S.T. Atomic Spectra Database, Website: <http://physics.nist.gov/cgi-bin/AtData/> (last accessed 4 February 2004).

⁴R. Schnabel, A. Bard, and M. Kock, Z. Tech. Phys. (Leipzig) **34**, 223 (1995).

⁵G. A. Martin, J. R. Fuhr, and W. L. Wiese, J. Phys. Chem. Ref. Data **17**, 1 (1988).

⁶A. A. Radzig and B. M. Smirnov, *Reference Data on Atoms, Molecules and Ions* (Springer-Verlag, Berlin, 1985).

⁷M. A. Collier, Ph.D. thesis, National University of Ireland Maynooth, 2004, document available on-line at <http://eprints.may.ie/archive/00000154/01/MartinCollierThesis.pdf>

⁸A. D. Kirkwood, K. D. Bier, J. K. Thompson, T. L. Haslett, A. S. Huber, and M. Moskovits, *J. Phys. Chem.* **95**, 2644 (1991).

⁹R. D. Cowan, *The Theory of Atomic Structure and Spectra*, (University of California Press, Berkeley, California, 1981), pp. 445–448.

¹⁰It is clear in the excitation spectra shown in Fig. 2, that the site labeling based on the z^6P state behavior is not consistent with that exhibited by the a^6D state in so far as both the excitation and emission of the blue site

occur at lower energies (590/626 nm) than the red site (585.7 nm). In the present case, the usage of the primary and secondary sites is the more appropriate, but since the red and blue site labeling has been established in the z^6P state work, this will be retained in this paper, despite it being formally incorrect for the a^6D state.

¹¹O. Byrne, M. A. Ryan, M. A. Collier, and J. G. McCaffrey, *J. Chem. Phys.* (to be published).